Journal of Molecular Catalysis A: Chemical 356 (2012) 20–28

Contents lists available at SciVerse ScienceDirect

Journal of Molecular Catalysis A: Chemical

journal homepage: www.elsevier.com/locate/molcata

Methane combustion activity of Pd–PdO_x–Pt/Al_2O_3 catalyst: The role of platinum promoter

Niko M. Kinnunen, Janne T. Hirvi, Mika Suvanto*, Tapani A. Pakkanen*

University of Eastern Finland, Department of Chemistry, P.O. Box 111, FI-80101 Joensuu, Finland

ARTICLE INFO

Article history:
Received 22 June 2011
Received in revised form
17 December 2011
Accepted 20 December 2011
Available online 31 December 2011

Keywords:
Methane
Combustion
Alumina
PdO
Pt
Pd

ABSTRACT

The effect of Pt promoter on Pd–PdO_x/Al_2O_3 catalyst was investigated to improve understanding of the role of promoter formation of the active phase of Pd–PdO_x–Pt/Al_2O_3 methane combustion catalysts. The influence of Pt addition on the composition of the active catalyst surface was characterized by NH_3 temperature programmed desorption procedure. Addition of promoter improved the low temperature CH_4 combustion activity of the aged catalyst, though it caused a decrease in activity of the fresh catalyst. The changes in activity were related to changes in the ratio of the metal to metal oxide phases in the surface composition. Pt tends to create metal sites, whereas Pd prefers the formation of metal oxide sites. Catalyst preparation parameters affect the Pd/PdO_x ratio of the non-promoted monometallic Pd catalyst, and the ratio needs to be known so that the proper amount of Pt promoter can be added.

1. Introduction

Natural gas and different blends of natural gas are of great interest nowadays in the effort to move toward less polluting transport fuels. Liquefied natural gas, which is natural gas in liquid form, contains methane as the main component. Methane is the most difficult of all hydrocarbons to oxidize completely [1] and it is a 20 times more potent greenhouse gas than CO_2 [2]. Moreover, high energy density of methane increases the combustion temperature, which causes more NO_x emissions. Other pollutants, such as unburned hydrocarbons (UHCs) and CO, are released simultaneously if the conditions at a running engine are unfavorable for complete oxidation [3,4]. A blend of compressed natural gas and hydrogen, called Hythane®, has been developed to reduce emissions particularly in heavy duty vehicles [4]. After-treatment of the exhaust gases is typically done in a three-way catalytic converter system consisting of oxidation and reduction catalysts where CO is oxidized to CO_2 and hydrocarbons (HCs) to H_2O and CO_2, while NO_x is reduced to N_2 and O_2 [5,6].

Catalysts for oxidation of CO and HCs consist of support material, active metal(s) and promoter(s). The support material has a high specific surface area to facilitate good dispersion of the active metal. It also increases the thermal stability of the metal [1]. Conventional support materials in methane combustion catalysts are alumina and zirconium oxides and their mixtures. Noble metals are applied as active metals [7–9], and platinum group metals have proved to be a good option for methane combustion [3,10,11]. Promoters improve catalytic activity [12–14], increase thermal stability of the support material [15,16], and retard sintering of active metal particles [17].

Platinum promoter has been shown to increase low temperature methane combustion activity and hinder the growth of Pd and PdO particle size [18] and crystallite size [19]. Small active metal cluster size has been linked to longer durability of the promoted catalyst in hydrocarbon combustion, but no correlation between particle size and methane combustion activity has been found for either the fresh or aged monometallic Pd–PdO_x catalysts [20,21]. Although too high Pt content suppresses the activity of the catalyst [22], no simple correlation has been indicated between the amount of Pt and methane combustion activity. The role of the Pt promoter is still unclear [19,22].

The methane combustion activity and thermal stability of the active metal particles can also be tailored without a promoter through proper choice of the active metal precursor and the impregnation solvent [20,21]. Support is thereby provided for a relationship between methane combustion activity of monometallic Pd–PdO_x catalysts and the ratio of metal (M) to metal oxide (MO_x). The target of the present study is to improve understanding of the effect of Pt promoter on active phase formation and particularly on the M/MO_x ratio of the alumina supported Pd–PdO_x catalyst. The reason for the improved thermal durability of the aged

* Corresponding authors. Tel.: +358 13 251 3312; fax: +358 13 251 3390.
E-mail addresses: Mika.Suvanto@uef.fi (M. Suvanto), Tapani.Pakkanen@uef.fi (T.A. Pakkanen).

1381-1169/$ – see front matter © 2011 Elsevier B.V. All rights reserved.
doi:10.1016/j.molcata.2011.12.023

Table 1
Compositions and preparation parameters of the catalysts.

Catalyst	Amount of active metal precursor (g)		Amount of active metals (mmol)		Total active metal loading (wt.%)	Impregnation time (h)	Volume of impregnation solution (cm^3)
	$Pd(acac)_2$	$Pt(acac)_2$	Pd	Pt			
Pd(24 h)	0.54	–	1.77	–	2.3	24	16
Pd(48 h)	0.54	–	1.77	–	2.3	48	16
Pd(72 h)	0.54	–	1.77	–	2.3	72	16
Pd(25 cm^3)	0.54	–	1.77	–	2.3	24	25
Pd(35 cm^3)	0.54	–	1.77	–	2.3	24	35
$Pd_{0.92}$–$Pt_{0.08}$[a]	0.54	0.06	1.77	0.15	2.6	24 + 24	16 + 16
$Pd_{0.85}$–$Pt_{0.15}$[a]	0.54	0.13	1.77	0.33	3.0	24 + 24	16 + 16
$Pd_{0.37}$–$Pt_{0.63}$[b]	0.17	0.38	0.56	0.97	3.0	24 + 24	16 + 16
Pt(2.3 wt.%)	–	0.38	–	0.97	2.3	24	16
Pt(4.1 wt.%)[c]	–	0.69	–	1.75	4.1	24	16

[a] Based on monometallic Pd(24 h) catalyst.
[b] Based on monometallic Pt(2.3 wt.%) catalyst.
[c] Pt mole fraction is the same as the Pd mole fraction of Pd(24 h) catalyst.

promoted Pd–PdO_x/Al_2O_3 catalyst is also of interest. The influence of parameters used in the preparation of monometallic Pd–PdO_x catalysts is discussed.

2. Experimental

Catalysts were prepared with alumina as a support material. The size distribution of alumina particles was <25 μm 37.8%, <45 μm 64.4%, and <90 μm 92.0%. The amount of support material was 8.0 g for each batch, and total active metal loading varied between 2.3 and 4.1 wt.%. The active metal precursors were $Pd(C_5H_7O_2)_2$ and $Pt(C_5H_7O_2)_2$, hereafter referred to as $Pd(acac)_2$ and $Pt(acac)_2$. Pure propionic acid (Fluka, p.a.) was diluted with water to prepare impregnation solution of 50 vol.% propionic acid–water solution (P50).

2.1. Catalyst preparation

Monometallic Pd catalysts with different preparation parameters and monometallic Pt catalysts with different loadings were prepared by wet impregnation method. Bimetallic catalysts were prepared by a stepwise impregnation method. In the stepwise impregnation, the catalyst undergoes the wet impregnation cycle twice to ensure controlled distribution and better contact between active metals [23]. The composition of the catalysts and details of the preparation are presented in Table 1.

2.1.1. Wet impregnation

The $Pd(acac)_2$ or $Pt(acac)_2$ was weighed into a 50-cm^3 flask and stirred with 10 cm^3 of impregnation solution. The alumina support was weighed in a weighing boat and slowly added to the active metal solution. The remaining impregnation solution was then added. The total amounts of impregnation solutions and impregnation times used in catalyst preparation are presented in Table 1. The impregnation solution was removed during the evaporation step by heating the flask at 313 K in a water bath. When the batch was completely dry, it was removed to a drying tray. The tray was placed in a furnace, where the batch was dried 10 h at 418 K. After drying, the batch was calcined under air for 2 h at 823 K. Half of the batch was aged under air for 4 h at 1173 K.

2.1.2. Stepwise impregnation

A stepwise method was used to prepare Pt promoted catalysts, $Pd_{0.92}$–$Pt_{0.08}$ and $Pd_{0.85}$–$Pt_{0.15}$, in which the monometallic Pd(24 h) catalyst was impregnated with promoter. The platinum precursor was dissolved in the P50 solution, which was heated in a water bath (T = 323 K), since heating improves solubility of the precursor and decreases the surface tension of the impregnation solution [24]. After 15 min mixing, freshly prepared and calcined Pd(24 h) catalyst was added slowly to the precursor solution. The mixture was stirred for 24 h. The impregnation solution was removed under vacuum by heating the flask in a water bath (T = 313 K). After evaporation, the catalyst was calcined and aged by the procedures described above (Section 2.1.1). The same stepwise procedure was used to prepare the $Pd_{0.37}$–$Pt_{0.63}$ catalyst with high Pt proportion, but now the Pd precursor was added to the Pt(2.3 wt.%) catalyst to avoid complete masking of the active Pd sites.

2.2. Characterization

Crystallinity and crystallite size of the active metal and metal oxide species were determined by powder X-ray diffraction (XRD). The XRD measurements were carried out with a *Bruker-AXD D8 Advance* device using Cu Kα as radiation source. The diffraction pattern was collected between 9° and 93° at 2θ scale with a step size of 0.11° min^{-1}. The crystallite sizes were evaluated from the diffraction data with TOPAS 2.0 software [25].

Dispersion was measured by CO chemisorption. The sample (~200 mg) was first pretreated under H_2 at a flow rate of 30 cm^3 min^{-1} and heated to 773 K at a heating rate of 20 K min^{-1}. Cooling to room temperature was carried out under helium at a flow rate of 30 cm^3 min^{-1}. The dispersion was then measured by CO pulse chemisorption at room temperature. The flow rate of helium during the chemisorption measurement was 10 cm^3 min^{-1}. Evaluation of the dispersion was carried out by GRAMS/32 software [26] by using a stoichiometric factor of 2 for Pd [27–30] and 1 for Pt.

Specific surface area of the catalyst was measured with a *Micromeritics ASAP 2010* device by Brunauer–Emmett–Teller method (BET). A sample (~200 mg) was pretreated in vacuum at 623 K for 2 h and the measurement was carried out at the temperature of liquid nitrogen. More specific surface characterization and identification of the concentrated active species were carried out with a *Hitachi S4800 FE-SEM*. Detailed surface analysis was done with a *Thermo Electron* EDS device. Working distance was 15 mm, accelerating voltage 20 kV, and current 20 μA.

Activity of the catalyst in methane combustion was measured under lean burn conditions. The test gas, produced by AGA, consisted of CH_4 (1%), O_2 (16%), and N_2 (83%). A catalyst sample of 600 mg was used. The activity performance was recorded three times for each catalyst, each time with a new sample. A detailed description of the methane combustion procedure and device can be found elsewhere [20,31]. Methane conversion rate (MCR)

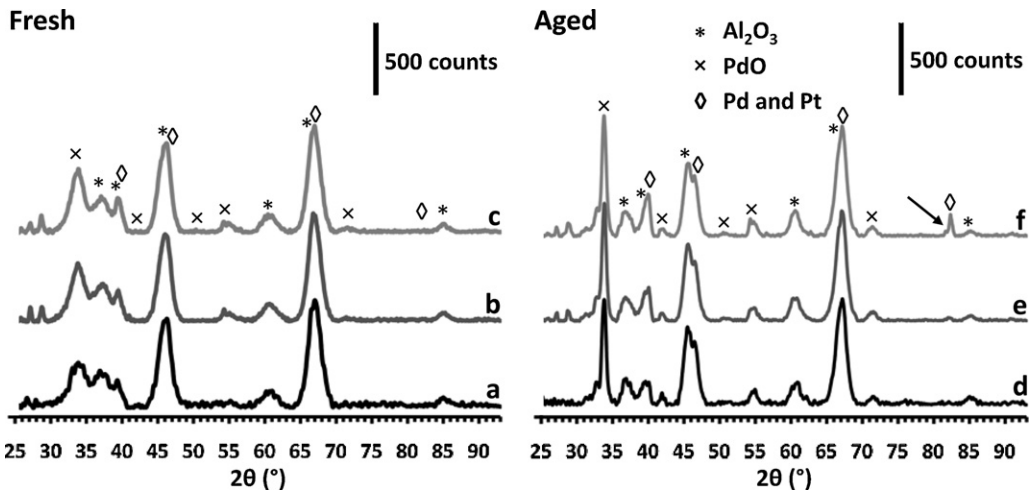

Fig. 1. XRD graphs of fresh (a) Pd(24 h), (b) $Pd_{0.92}$–$Pt_{0.08}$, and (c) $Pd_{0.85}$–$Pt_{0.15}$ catalysts and aged (d) Pd(24 h), (e) $Pd_{0.92}$–$Pt_{0.08}$, and (f) $Pd_{0.85}$–$Pt_{0.15}$ catalysts.

[$mol_{CH_4}\ g_{Pd}^{-1}\ s^{-1}$] based on mass of the active metal (M) was calculated by Eq. (1):

$$\mathrm{MCR} = \frac{((X_{CH_4}/100) \times 8.17 \times 10^{-6}\ \mathrm{mol}_{CH_4}\ \mathrm{s}^{-1})}{m_M} \quad (1)$$

where X_{CH_4} is methane conversion at the measurement temperature [%], $8.17 \times 10^{-6}\ mol_{CH_4}\ s^{-1}$ is the total methane flow rate per second, and m_M is the mass of active metal [g]. Turnover rate (TOR) [s^{-1}] was calculated by Eq. (2):

$$\mathrm{TOR} = \frac{((X_{CH_4}/100) \times 8.17 \times 10^{-6}\ \mathrm{mol}\ _{CH_4}\ \mathrm{s}^{-1})}{((D_M/100) \times n_M)} \quad (2)$$

where D_M is active metal dispersion [%] and n_M is the amount of active metal [mol].

Thermal stability of the bulk active metal oxides was studied by temperature programmed oxidation (TPO). Catalyst samples were not pretreated. The measurement was carried out under gas mixture of He (20 $cm^3\ min^{-1}$) and O_2 (3 $cm^3\ min^{-1}$). The TPO curve was recorded while the catalyst was heated at a rate of 20 K min^{-1} from 303 K to 1323 K. Before recording of the data, the signal was stabilized for 18 min. During the measurement, a cold trap (T = 213 K) was used to remove water vapor. The composition of the desorbing gas, below 500 K, was identified with a Hewlett-Packard gas chromatograph.

Characterization of acid sites of the catalyst was carried out by temperature programmed ammonia desorption (NH_3 TPD), which is a quantitative method [32]. However, the present NH_3 TPD results are reported and compared at a semi-quantitative level, as in our previous work [21], because the exact composition of the desorbing gas was unknown. An Autochem 2100 device was utilized for the TPD measurements. A sample of 150 mg was heated to 823 K (20 K min^{-1}) under helium at a flow rate of 30 $cm^3\ min^{-1}$. After cooling, NH_3 gas was introduced to the catalyst, using 10 vol.% blend of NH_3 and He gas (20 $cm^3\ min^{-1}$) at 313 K for 1 h. Physically adsorbed NH_3 was removed by flushing the sample with helium (20 $cm^3\ min^{-1}$) for 1 h. Finally, the sample was heated at 10 K min^{-1} from 313 K to 823 K to record the NH_3 desorption curve. Integration of the peaks was carried out using GRAMS/32 program [26]. The ammonia desorption results were confirmed with XPS measurements (ESCA3000, VG Microtech Inc., UK) of fresh and aged Pd(24 h) and fresh Pt(4.1 wt.%) catalysts. The XPS spectra were recorded before and after annealing treatment at 823 K for 1 h under vacuum, which simulates the pretreatment of the NH_3 TPD measurement. The binding energy region around 335 eV has been considered.

3. Results and discussion

3.1. Characterization by XRD, CO chemisorption and BET methods

The effect of Pt promoter addition on the X-ray diffraction pattern of the Pd–PdO_x/Al_2O_3 catalyst and the characteristic reflections of the metallic Pd and Pt, PdO, and alumina support are presented in Fig. 1. No reflections for platinum oxides were observed. Diffraction patterns of the five monometallic Pd–PdO_x/Al_2O_3 catalysts were similar to each other and also to those of our previous study [21]. Addition of Pt promoter causes a new reflection at 2θ scale of 82° on the aged catalyst (marked with an arrow in Fig. 1). Clear shoulders at 40° and 46° can be seen. The intensities of the corresponding peaks increase with the amount of Pt promoter and hence can be attributed to metallic platinum. As is clear from Fig. 2, neither crystalline PtO nor PtO_2 phase was present for the monometallic Pt catalysts, indicating that the Pt exists only in metallic form. Fig. 2 also suggests that a high proportion of Pt influences the ratio of the Pd and PdO phases, for the PdO peaks do not appear for the $Pd_{0.37}$–$Pt_{0.63}$ catalyst.

The PdO crystallite size was evaluated from the characteristic peak at 2θ scale of 34° and Pt crystallite size from the peak at 82°. The results in Table 2 indicate that neither the impregnation parameters nor the promoter affect the PdO crystallite size of the fresh or aged catalysts. Earlier, the introduction of Pt promoter was found to increase slightly the crystallite size of PdO [22]. In contrast, the Pt crystallite size of the aged bimetallic catalysts was clearly smaller than that of the monometallic Pt catalysts. We note, however, that the particles may consist of multiple crystalline domains, and the particle and crystallite sizes are not necessarily comparable [33].

As can be seen in Table 2, the dispersions of active metal are between 23.5% and 46.6% for the fresh catalysts and between 2.3% and 11.7% for the aged catalysts. The preparation parameters do not affect the dispersion of the monometallic Pd–PdO_x/Al_2O_3 catalysts. Moreover, the bimetallic fresh and aged catalysts exhibit similar active metal dispersion to the fresh and aged monometallic Pd–PdO_x catalysts. However, dispersion of the monometallic Pt catalysts drops dramatically with aging. In contrast to our result, Castellazzi et al. [22] observed the addition of Pt promoter to decrease the dispersion of the active phase. BET surface areas of fresh catalysts (Table 2) are about 210 $m^2\ g^{-1}$ and those of the aged catalysts about 150 $m^2\ g^{-1}$. The decrease in BET surface area during aging is due to the high temperature and gas atmosphere. The surface areas of the support material [34] and the catalysts [35]

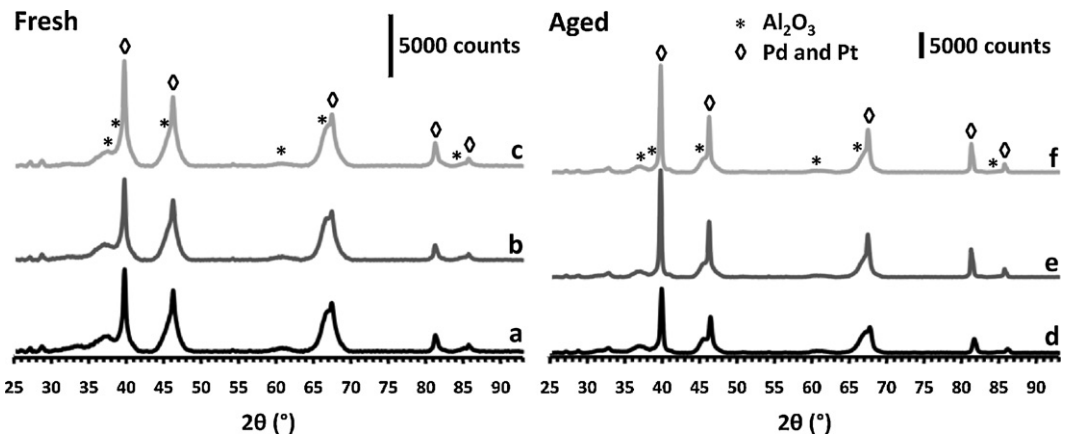

Fig. 2. XRD graphs of fresh (a) $Pd_{0.37}$–$Pt_{0.63}$, (b) Pt(2.3 wt.%), and (c) Pt(4.1 wt.%) catalysts and aged (d) $Pd_{0.37}$–$Pt_{0.63}$, (e) Pt(2.3 wt.%), and (f) Pt(4.1 wt.%) catalysts. Note the difference in scale bars.

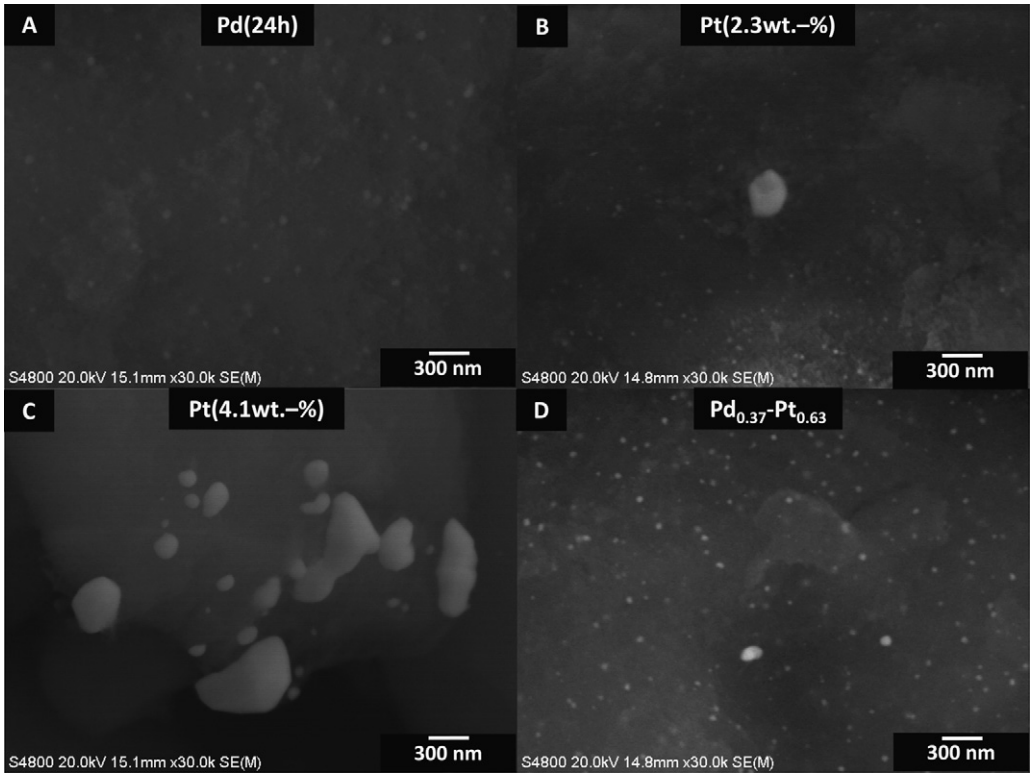

Fig. 3. SEM images (×30,000) of the aged (A) Pd(24 h), (B) Pt(2.3 wt.%), (C) Pt(4.1 wt.%), and (D) $Pd_{0.37}$–$Pt_{0.63}$ catalysts.

Table 2
PdO and Pt crystallite sizes, active metal dispersions, and BET surface areas of the studied catalysts.

Catalyst	PdO crystallite size (nm)		Pt crystallite size (nm)		Active metal dispersion (%)		BET surface area ($m^2\ g^{-1}$)	
	Fresh	Aged	Fresh	Aged	Fresh	Aged	Fresh	Aged
Pd(24 h)	2.7	12.9	–	–	25.6	11.7	206	148
Pd(48 h)	3.1	14.7	–	–	26.6	9.2	216	150
Pd(72 h)	3.2	15.9	–	–	23.5	7.8	214	143
Pd(25 cm^3)	3.0	14.5	–	–	25.7	8.5	211	141
Pd(35 cm^3)	3.1	14.7	–	–	26.7	10.1	211	166
$Pd_{0.92}$–$Pt_{0.08}$	3.4	12.1	n.d.[a]	32.4	27.4	12.1	202	151
$Pd_{0.85}$–$Pt_{0.15}$	3.3	12.6	n.d.[a]	36.5	24.2	9.5	210	144
$Pd_{0.37}$–$Pt_{0.63}$	n.d.[a]	n.d.[a]	35.9	43.2	29.0	11.6	213	142
Pt(2.3 wt.%)	–	–	33.9	68.3	24.0	4.2	211	145
Pt(4.1 wt.%)	–	–	30.8	74.8	46.6	2.3	212	146

[a] No peak was detected.

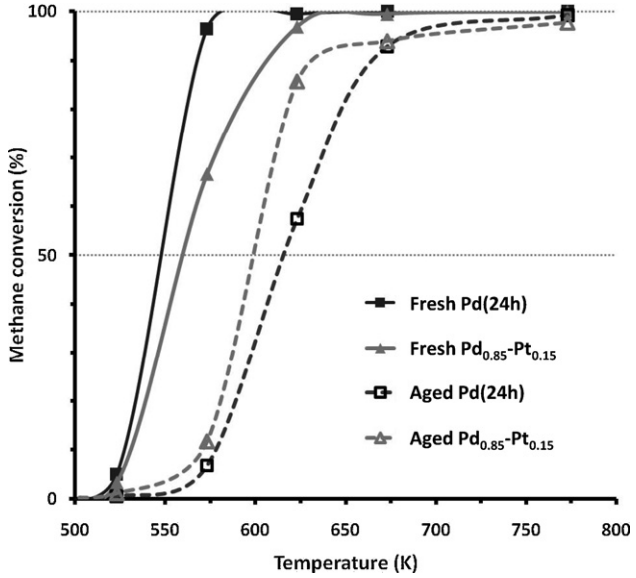

Fig. 4. Methane conversion curves of the fresh (solid lines) and aged (dashed lines) Pd(24 h) and $Pd_{0.85}$–$Pt_{0.15}$ catalysts.

decrease considerably more in aging under oxidizing conditions than under reducing conditions.

3.2. SEM/EDS characterization

The support material of the catalysts consisted of nano- and microsized alumina particles. The SEM studies indicated that long impregnation time (72 h) may decrease the particle size of the microsized support, whereas the amount of impregnation solution has no effect. Fig. 3 presents SEM images of the microsized support particles of the aged monometallic Pd(24 h), Pt(2.3 wt.%), Pt(4.1 wt.%) and bimetallic $Pd_{0.37}$–$Pt_{0.63}$ catalysts. Maintenance of dispersion is an important property. Inspection of Fig. 3A and B shows how aging increases the particle size of the different active metals at equal metal loadings (2.3 wt.%). The growth of Pt metal particles is still clearer in a comparison of catalysts with equal

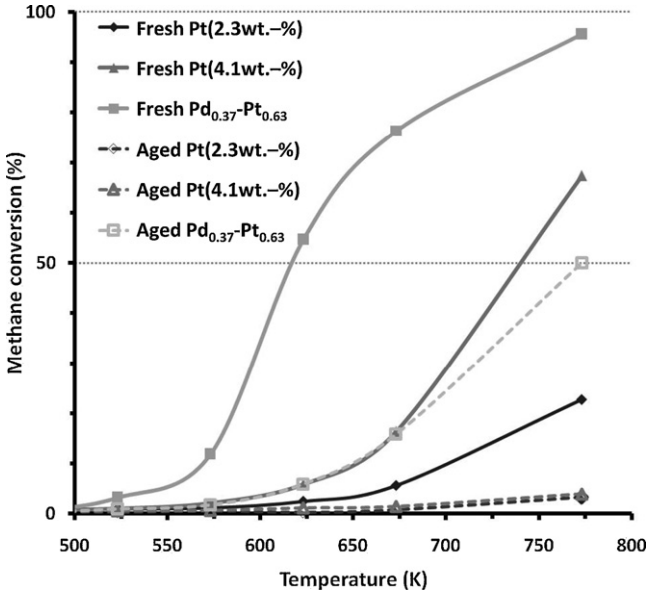

Fig. 5. Methane conversion curves of the fresh (solid lines) and aged (dashed lines) Pt(2.3 wt.%), Pt(4.1 wt.%), and $Pd_{0.37}$–$Pt_{0.63}$ catalysts.

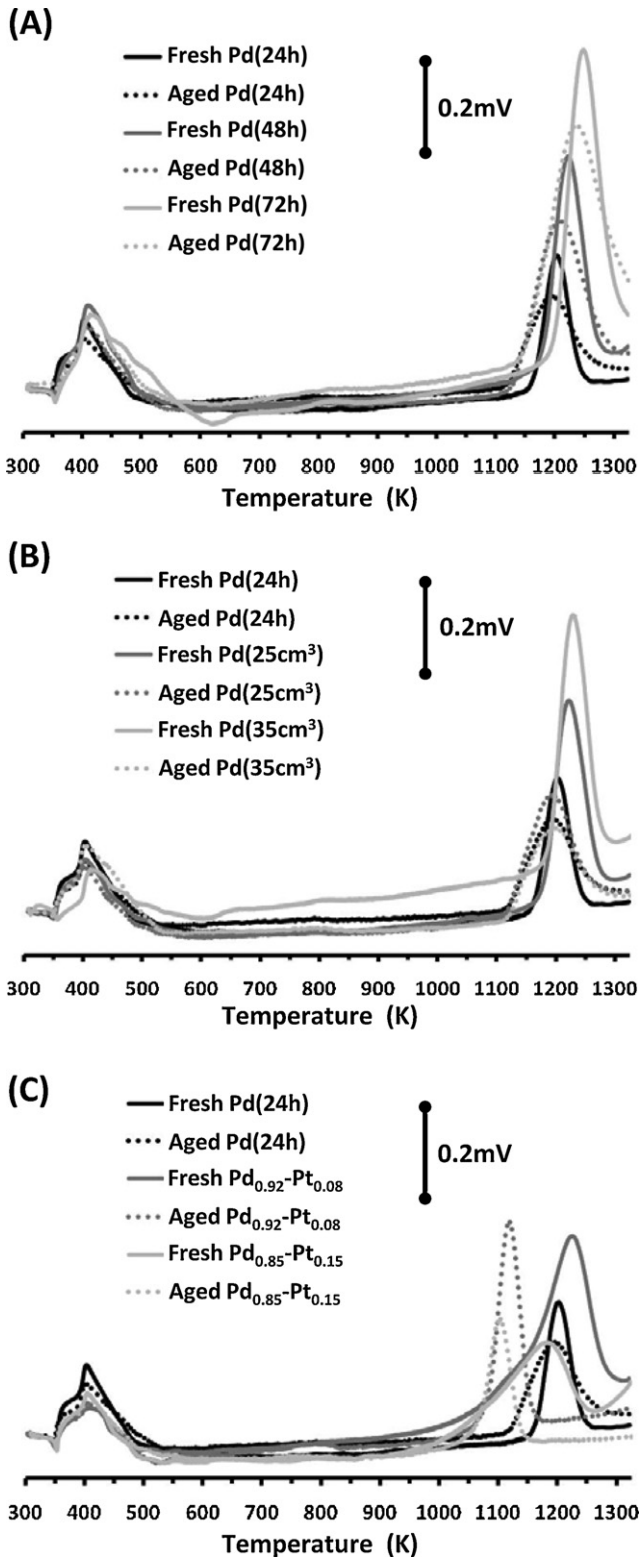

Fig. 6. Effect of (A) impregnation time, (B) volume of impregnation solvent, and (C) Pt promoter on TPO profiles of the fresh (solid lines) and aged (dotted lines) catalysts.

metal mole fractions (Fig. 3A and C). Large Pt-rich particles were confirmed by EDS. In general, alumina-supported Pt catalysts were fairly unstable in aging. However, Fig. 3D shows that the growth of particles is hindered in the bimetallic catalyst even when the

proportion of Pt is large. These observations are in good agreement with our dispersion results (Table 2).

3.3. Methane combustion activity

Methane conversion curves for the fresh and aged Pd(24 h) and $Pd_{0.85}$–$Pt_{0.15}$ catalysts are compared in Fig. 4. Activity is better for the aged Pt promoted $Pd_{0.85}$–$Pt_{0.15}$ catalyst than for the aged monometallic Pd(24 h) catalyst, showing that Pt promoter improves the durability of the catalyst. The conversion profiles of the fresh catalysts show the reverse order. Activities of the fresh and aged $Pd_{0.37}$–$Pt_{0.63}$ catalysts, with high Pt proportion, are notably lower than the activities of the $Pd_{0.85}$–$Pt_{0.15}$ (cf. Figs. 4 and 5) and other bimetallic catalysts. In fact, like both the fresh and aged Pt(2.3 wt.%) and Pt(4.1 wt.%) catalysts, the aged $Pd_{0.37}$–$Pt_{0.63}$ catalyst is inactive below 623 K (Fig. 5). This is an interesting finding, since the active metal dispersion of the aged $Pd_{0.37}$–$Pt_{0.63}$ is clearly higher than that of the monometallic Pt catalysts (see Table 2). Evidently dispersion is not necessarily the dominant factor for low temperature activity in methane combustion.

Table 3 summarizes methane light-off temperatures, methane conversions, methane conversion rates (MCR), and turnover rates (TOR) of the catalysts. The best TOR values are achieved for the fresh monometallic Pd–PdO_x catalysts. The values are slightly better than those reported in the literature [36,37] and in agreement with our previous results [21]. The impregnation parameters do not have a significant effect on the TORs. The turnover rates of the fresh and aged monometallic Pt catalysts are low, as expected, since Pt is a less active metal in methane combustion [42]. The fresh $Pd_{0.92}$–$Pt_{0.08}$ and $Pd_{0.85}$–$Pt_{0.15}$ catalysts exhibit TORs between those of the monometallic Pd–PdO_x and Pt catalysts, whereas the aged $Pd_{0.85}$–$Pt_{0.15}$ catalyst exhibits highest activity of all the aged catalysts.

3.4. Thermal stability of active species

TPO profiles of the supported monometallic and Pt-promoted Pd–PdO_x catalysts include two desorption peaks (Fig. 6). The first peak occurs between 350 K and 550 K and is due to the desorption of O_2 [38,39]. Our gas chromatograph analysis showed the desorbing gas to contain CO_2 as well. The presence of CO_2 is observed because the sample is stored under air and CO_2 binds to the acid sites of the catalyst. The second desorption peak is due to the thermal decomposition of PdO to metallic Pd, which is reported generally to occur between 973 K and 1173 K [38,40,41]. According to Gélin and Primet [42], PdO is stable up to 1073 K in air under normal pressure, whereas the most stable platinum oxide (PtO_2) under similar conditions decomposes at 673 K.

The maximum of the PdO decomposition peak for the monometallic Pd–PdO_x catalysts lies between 1200 K and 1300 K. The change in the peak position may be due to high O_2 concentration of the measurement gas mixture or to strong metal–support interaction [43]. An increase in impregnation time improves the thermal stability of the both fresh and aged catalysts (Fig. 6A). The improvement in thermal stability of PdO can be explained by the progress of reaction between carboxylic acid, aluminum oxide and palladium precursor [44]. Increase in the volume of impregnation solution also increases the thermal stability of the fresh catalysts, but not that of the aged catalysts (Fig. 6B). After addition of the Pt promoter, the thermal decomposition peak of oxide of the fresh catalysts becomes broader, and the maximum appears between 1150 K and 1250 K (Fig. 6C). With aging, the maximum of the peak moves noticeably toward lower temperature and sharpens, as was also observed earlier [22]. An increase in the amount of Pt causes a decrease in the area of the decomposition peak, which corresponds to the smaller amount of the oxide. The monometallic Pt catalysts and the $Pd_{0.37}$–$Pt_{0.63}$ catalyst with high Pt proportion do not show the thermal decomposition peak of the oxide.

3.5. Determination of active sites

The NH_3 TPD profiles of noble metal catalysts show three peaks corresponding to desorption from alumina, metal oxide (MO_x), and metal (M) sites (Fig. 7). Table 4 summarizes the peak integrals and calculated M/MO_x ratios obtained by NH_3 TPD and XPS methods. Although the preparation parameters affect the M/MO_x ratio in some degree, no clear trends are evident, at least not for the fresh catalysts. Small differences in homogeneity and calcination of the catalysts may screen the effects for the fresh catalysts. A slight trend in the M/MO_x ratios can be seen after aging.

The effect of Pt promoter on the NH_3 TPD profile of the fresh Pd–PdO_x catalyst (Pd(24 h)) is presented in Fig. 7. Addition of Pt increases the integral of the last broad desorption peak related to the metal (M) sites. This is in agreement with the finding that the fresh and aged monometallic Pt catalysts show only a peak for metallic Pt (Fig. 8). Furthermore, XPS measurement of the fresh Pt(4.1 wt.%) catalyst after the thermal treatment at 823 K gives no indication for the existence of PtO_x. In general, the M/MO_x ratio is highest for the catalyst with highest Pt proportion. The effect of aging on the NH_3 TPD profiles of the catalysts is shown in Figs. 7 and 8. Previously we have concluded that low temperature activity in methane combustion decreases with aging because the relative amount of PdO_x sites increases and thus the M/MO_x ratio decreases [21]. The observation is also supported by the present XPS data shown in Fig. 9. The same conclusion can be drawn for the bimetallic catalysts, though addition of Pt promoter may in fact lead to slightly higher M/MO_x ratio by sustaining the metallic form. As an extreme, the high proportion of Pt in the $Pd_{0.37}$–$Pt_{0.63}$ catalyst seems to prevent the re-oxidation of palladium, as was earlier suggested for Pt-promoted Pd catalysts in general [22]. Comparison of the NH_3 desorption curves in Fig. 8 shows the MO_x related peak to exist for the fresh $Pd_{0.37}$–$Pt_{0.63}$ catalyst, but it disappears during aging.

3.6. Active phase of methane combustion catalyst

Coexistence of metallic Pd and PdO_x has been observed on methane combustion catalysts [45,46]. Several groups also suggest that the simultaneous presence of these phases is essential for formation of the active catalyst in CH_4 oxidation [37,47,48]. We observed earlier for the monometallic Pd catalyst that low temperature methane combustion activity correlates with the Pd/PdO_x ratio [21]. We concluded, moreover, that an important reason for the loss of activity under oxidizing aging conditions is decrease in the number of metal sites. In the present study, the negative effect of aging was successfully reduced through addition of the Pt promoter. As also indicated by our XRD, TPO, and NH_3 TPD results, platinum is hard to oxidize and it remains in metallic state even under oxidizing conditions [42]. We conclude that the addition of Pt increases the number of metal sites and slightly improves the low temperature activity of the catalyst because of the larger M/MO_x ratio. Overall, platinum provides metal sites, whereas palladium is responsible for both metal and metal oxide sites, and the number of PdO_x sites increases noticeably during aging.

Fig. 10 shows correlation between TOR and the M/MO_x ratio. As is evident, the active form of the Al_2O_3-supported Pd–PdO_x catalyst contains both metal and metal oxide phases, and good low temperature methane combustion activity is achieved with proper M/MO_x ratio. The results show as well that combustion activity decreases with too high M/MO_x ratio. Such activity behavior can be explained by the lower activity of metallic Pd and Pt than of MO_x in low temperature methane combustion [43,49]. The M/MO_x ratio

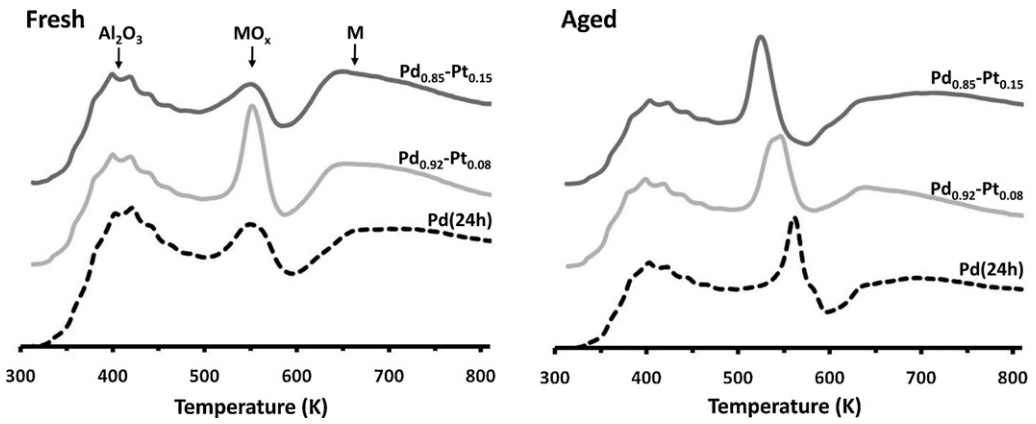

Fig. 7. NH_3 TPD curves of the fresh and aged monometallic Pd(24 h) and bimetallic $Pd_{0.92}$–$Pt_{0.08}$ and $Pd_{0.85}$–$Pt_{0.15}$ catalysts.

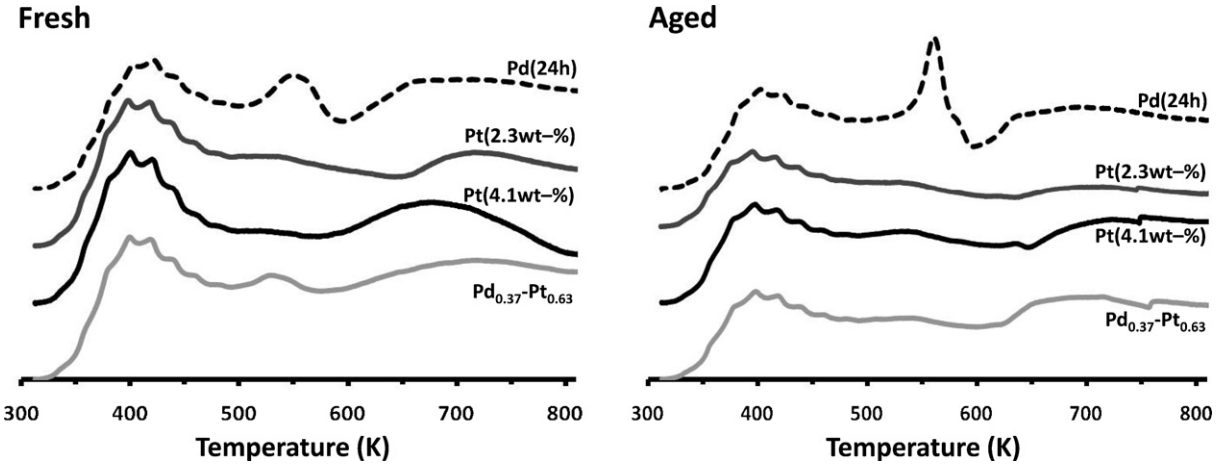

Fig. 8. NH_3 TPD curves of fresh and aged monometallic Pd(24 h), Pt(2.3 wt.%), and Pt(4.1 wt.%) catalysts and the bimetallic $Pd_{0.37}$–$Pt_{0.63}$ catalyst.

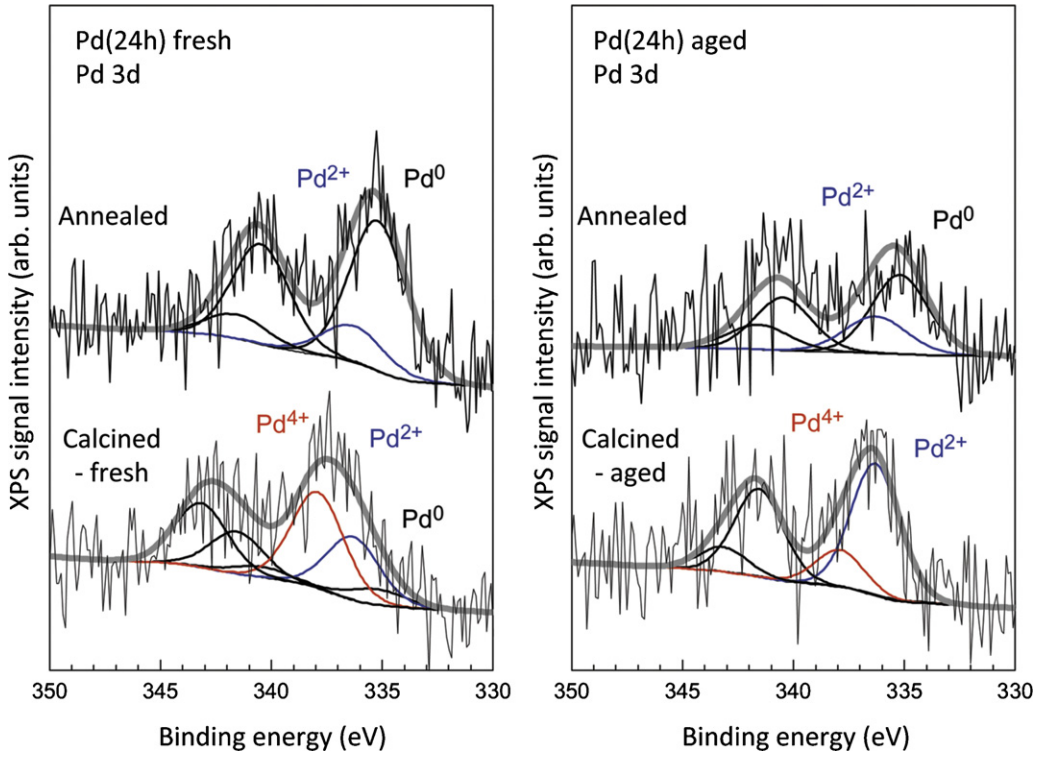

Fig. 9. XPS spectra and oxidation states of fresh and aged monometallic Pd(24 h) catalysts.

Table 3
Methane light-off temperatures together with methane conversions, methane conversion rates (MCRs), and turnover rates (TORs) at 573 K for the catalysts.

Catalyst	Light-off temperature (K)		Light-off difference (K)	Methane conversion (%)		MCR (μmol g_M^{-1} s^{-1})		TOR ($\times 10^{-2}$ s^{-1})	
	Fresh	Aged		Fresh	Aged	Fresh	Aged	Fresh	Aged
Pd(24 h)	548	610	62	96.0	6.6	566	39	23.5	3.5
Pd(48 h)	552	622	70	79.0	5.9	465	35	18.7	4.0
Pd(72 h)	555	633	78	72.3	6.0	426	35	19.3	4.8
Pd(25 cm^3)	547	614	67	94.1	5.5	555	32	23.0	4.0
Pd(35 cm^3)	549	620	71	89.1	5.8	525	34	20.9	3.6
$Pd_{0.92}$–$Pt_{0.08}$	556	613	57	71.6	8.9	368	46	14.7	4.1
$Pd_{0.85}$–$Pt_{0.15}$	559	598	39	66.6	11.7	301	53	14.2	6.4
$Pd_{0.63}$–$Pt_{0.37}$	617	773	156	12.0	1.8	53	8	2.6	1.0
Pt(2.3 wt.%)	n.d.[a]	n.d.[a]	–	1.2	0.7	7	4	0.3	1.0
Pt(4. 1 wt.%)	740	n.d.[a]	–	2.1	0.7	7	2	0.3	1.9

[a] No methane light-off was observed at measurement temperatures between 298 K and 773 K.

Table 4
Integrals and calculated M/MO_x ratios of the fresh and aged catalysts obtained by NH_3 desorption and XPS methods.

Catalyst	Fresh catalysts			Aged catalysts		
	M	MO_x	M/MO_x ratio	M	MO_x	M/MO_x ratio
Pd(24 h)	2.08 (0.20)[a]	0.89 (0.05)[a]	2.34 (4.00)[a]	1.59 (0.11)[a]	1.40 (0.05)[a]	1.13 (2.20)[a]
Pd(48 h)	1.53	0.74	2.07	1.32	1.58	0.83
Pd(72 h)	1.58	0.47	3.37	1.42	1.76	0.81
Pd(25 cm^3)	1.99	0.92	2.16	1.22	1.30	0.92
Pd(35 cm^3)	1.63	0.58	2.81	1.23	1.67	0.74
$Pd_{0.92}$–$Pt_{0.08}$	3.12	1.58	1.97	1.28	1.12	1.15
$Pd_{0.85}$–$Pt_{0.15}$	3.58	0.94	3.83	2.09	1.49	1.40
$Pd_{0.37}$–$Pt_{0.63}$	1.64	0.33	4.95	1.29	n.d.[b]	–[c]
Pt(2.3 wt.%)	0.83	n.d.[b]	–[c]	0.51	n.d.[b]	–[c]
Pt(4.1 wt.%)	1.74	n.d.[b]	–[c]	0.89	n.d.[b]	–[c]

[a] The at.% values, presented in parentheses, were obtained by deconvolution from XPS spectra presented in Fig. 9.
[b] No corresponding peak was detected.
[c] Not calculated, since data was incomplete.

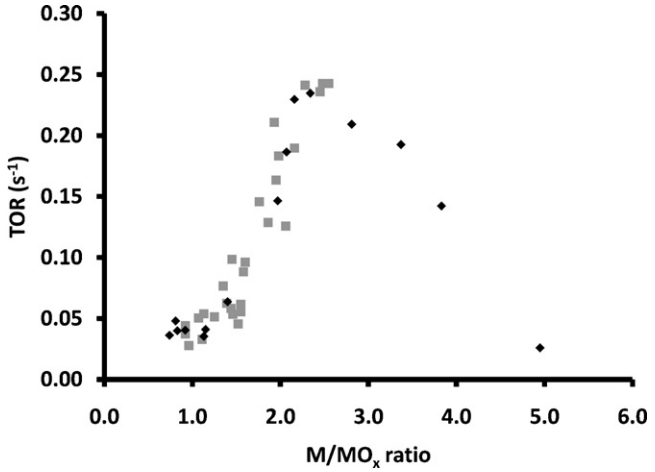

Fig. 10. Turnover rates (TORs) as a function of M/MO_x ratio. The results shown as gray squares are included for comparison [21].

of the non-promoted monometallic catalyst needs to be known in order that the proper proportion of promoter can be added.

4. Conclusions

The effects of preparation parameters and Pt promoter on monometallic Pd–PdO_x catalysts were studied. Aging durability of the catalyst was successfully improved by adding the promoter. In general, the activity was related to the proportions of metal (M) and metal oxide (MO_x) surface sites, allowing the following conclusions to be drawn:

- The active phase of the catalyst for low temperature CH_4 combustion contains both M and MO_x forms.
- The preparation parameters of the monometallic base catalyst influence the M/MO_x ratio, but no clear trends were observed.
- The platinum promoter prefers metallic form, while palladium exists in both metallic and oxide forms.
- The M/MO_x ratio decreases in aging due to the formation of stable PdO, but the addition of Pt improves the ratio by increasing the number of M sites and thus enhances the low temperature activity.
- Re-oxidation of palladium is prevented at high platinum proportions, and this is reflected in a loss of low temperature CH_4 combustion activity.

Acknowledgment

Ecocat Oy is thanked for supplying the alumina support material.

References

[1] A.K. Neyestanaki, F. Klingstedt, T. Salmi, D.Y. Murzin, Fuel 83 (2004) 395–408.
[2] R.E. Hayes, Chem. Eng. Sci. 59 (2004) 4073–4080.
[3] G. Centi, J. Mol. Catal. A 173 (2001) 287–312.
[4] L.A. Graham, G. Rideout, D. Rosenblatt, J. Hendren, Atmos. Environ. 42 (2008) 4665–4681.
[5] J. Kašpar, P. Fornasiero, N. Hickey, Catal. Today 77 (2003) 419–449.
[6] R. Di Monte, J. Kašpar, Top. Catal. 1–4 (2004) 47–57.
[7] V.R. Choudhary, V.P. Patil, P. Jana, B.S. Uphade, Appl. Catal. A 350 (2008) 186–190.
[8] R.J.H. Grisel, P.J. Kooyman, B.E. Nieuwenhuys, J. Catal. 191 (2000) 430–437.
[9] J.H. Lee, D.L. Trimm, Fuel Process. Technol. 42 (1995) 339–359.
[10] P. Gélin, L. Urfels, M. Primet, E. Tena, Catal. Today 83 (2003) 45–57.
[11] J.K. Lampert, M.S. Kazi, R.J. Farrauto, Appl. Catal. B 14 (1997) 211–233.
[12] Y. Yazawa, H. Yoshida, S.-i. Komai, T. Hattori, Appl. Catal. A 233 (2002) 113–124.
[13] B. Yue, R. Zhou, Y. Wang, X. Zheng, Appl. Catal. A 295 (2005) 31–39.
[14] T. Kolli, K. Rahkamaa-Tolonen, U. Lassi, A. Savimäki, R.L. Keiski, Catal. Today 100 (2005) 303–307.

[15] B. Ersoy, V. Gunay, Ceram. Int. 30 (2004) 163–170.
[16] O.V. Mokhnachuk, S.O. Soloviev, A.Y. Kapran, Catal. Today 119 (2007) 145–151.
[17] Y. Ozawa, Y. Tochihara, A. Watanabe, M. Nagai, S. Omi, Appl. Catal. A 258 (2004) 261–267.
[18] K. Narui, H. Yata, K. Furuta, A. Nishida, Y. Kohtoku, T. Matsuzaki, Appl. Catal. A 179 (1999) 165–173.
[19] H. Yamamoto, H. Uchida, Catal. Today 45 (1998) 147–151.
[20] N.M. Kinnunen, M. Suvanto, M.A. Moreno, A. Savimäki, K. Kallinen, T.-J.J. Kinnunen, T.A. Pakkanen, Appl. Catal. A 307 (2009) 78–87.
[21] N.M. Kinnunen, J.T. Hirvi, T. Venäläinen, M. Suvanto, T.A. Pakkanen, Appl. Catal. A 397 (2011) 54–61.
[22] P. Castellazzi, G. Groppi, P. Forzatti, Appl. Catal. B 95 (2010) 303–311.
[23] M. Rassoul, F. Gaillard, E. Garbowski, M. Primet, J. Catal. 203 (2001) 232–241.
[24] E. Álvarez, G. Vázquez, M. Sánchez-Vilas, B. Sanjurjo, J.M. Navaza, J. Chem. Eng. Data 42 (1997) 957–960.
[25] Bruker AXS, TOPAS V2.0: General Profile Analysis Software for Powder Diffraction Data, in: User Manual, Bruker AXS, Karlsruhe, Germany, 2000.
[26] GRAMS/32, v4.0, Galactic Industries Corporation.
[27] S.D. Jackson, L.A. Shaw, Appl. Catal. A 134 (1996) 91–99.
[28] C.A. Müller, M. Maciejewski, R.A. Koeppel, A. Baiker, Catal. Today 47 (1999) 245–252.
[29] G. Fagherazzi, P. Canton, P. Riello, N. Pernicone, F. Pinna, M. Battagliarin, Langmuir 16 (2000) 4539–4546.
[30] P. Canton, G. Fagherazzi, M. Battagliarin, F. Menegazzo, F. Pinna, N. Pernicone, Langmuir 18 (2002) 6530–6535.
[31] M.J. Koponen, T. Venäläinen, M. Suvanto, K. Kallinen, T.-J.J. Kinnunen, M. Härkönen, T.A. Pakkanen, J. Mol. Catal. A 258 (2006) 246–250.
[32] A. Corma, Chem. Rev. 95 (1995) 559–614.
[33] R.E. Dinnebier, S.J.L. Billinge (Eds.), Powder Diffraction: Theory and Practice, RSC Publishing, Cambridge, UK, 2008.
[34] A. Piras, A. Trovarelli, G. Dolcetti, Appl. Catal. B 28 (2000) L77–L81.
[35] U. Lassi, R. Polvinen, S. Suhonen, K. Kallinen, A. Savimäki, M. Härkönen, M. Valden, R.L. Keiski, Appl. Catal. A 263 (2004) 241–248.
[36] G. Zhu, K.-i. Fujimoto, D.Y. Zemlyanov, A.K. Datye, F.H. Ribeiro, J. Catal. 225 (2004) 170–178.
[37] K.-i. Fujimoto, F.H. Ribeiro, M. Avalos-Borja, E. Iglesia, J. Catal. 179 (1998) 431–442.
[38] R. Zhou, B. Zhao, B. Yue, Appl. Surf. Sci. 254 (2008) 4701–4707.
[39] B. Zhao, C. Yang, Q. Wang, G. Li, R. Zhou, J. Alloys Compd. 494 (2010) 340–346.
[40] K. Persson, P.O. Thevenin, K. Jansson, J. Agrell, S.G. Järås, L.J. Pettersson, Appl. Catal. A 249 (2003) 165–174.
[41] G. Lapisardi, L. Urfels, P. Gélin, M. Primet, A. Kaddouri, E. Garbowski, S. Toppi, E. Tena, Catal. Today 117 (2006) 564–568.
[42] P. Gélin, M. Primet, Appl. Catal. B 39 (2002) 1–37.
[43] G. Groppi, C. Cristiani, L. Lietti, P. Forzatti, Stud. Surf. Sci. Catal. 130 (2000) 3801–3806.
[44] D. Wickham, R. Cook, United States Patent Application Publication, Pub. No.: US 2003/0,176,278 A1.
[45] A.K. Datye, J. Bravo, T.R. Nelson, P. Atanasova, M. Lyubovsky, L. Pfefferle, Appl. Catal. A 198 (2000) 179–196.
[46] S. Colussi, A. Trovarelli, G. Groppi, J. Llorca, Catal. Commun. 8 (2007) 1263–1266.
[47] D. Gao, C. Zhang, S. Wang, Z. Yuan, S. Wang, Catal. Commun. 9 (2008) 2583–2587.
[48] Y. Yazawa, H. Yoshida, N. Takagi, S.-i. Komai, A. Satsuma, T. Hattori, Appl. Catal. B 19 (1998) 261–266.
[49] R. Burch, F.J. Urbano, Appl. Catal. A 124 (1995) 121–138.